Electronic Supplementary Material (ESI) for Sustainable Energy & Fuels.
This journal is © The Royal Society of Chemistry 2019

Supplementary Information

Ultra-fast shock-wave combustion synthesis of nanostructured silicon from sand with excellent Li storage performance

Ali Reza Kamali*, Safa Haghighat-Shishavan, Masoud Nazarian-Samani, Asma Rezaei, Kwang-Bum Kim

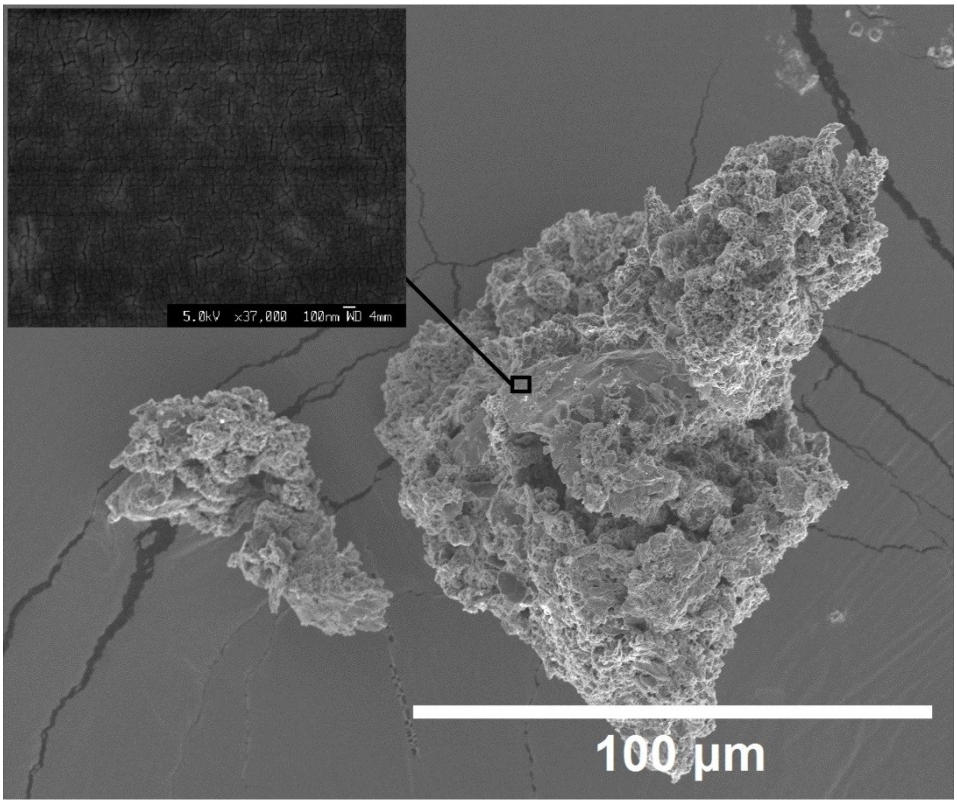

Fig. S1. SEM micrograph of the ball-milled sand after being heated with $KClO_4$ in the thermal analysis equipment. The inset is a higher magnification SEM micrograph from the area indicated in the main micrograph.

The morphological features of the mesoporous Si produced in this study have been demonstrated in Fig. 2 and Fig. S2. The product is comprised of particles with various sizes less than 200 μm with a nanostructured interconnected sheet-like morphology with high porosity.

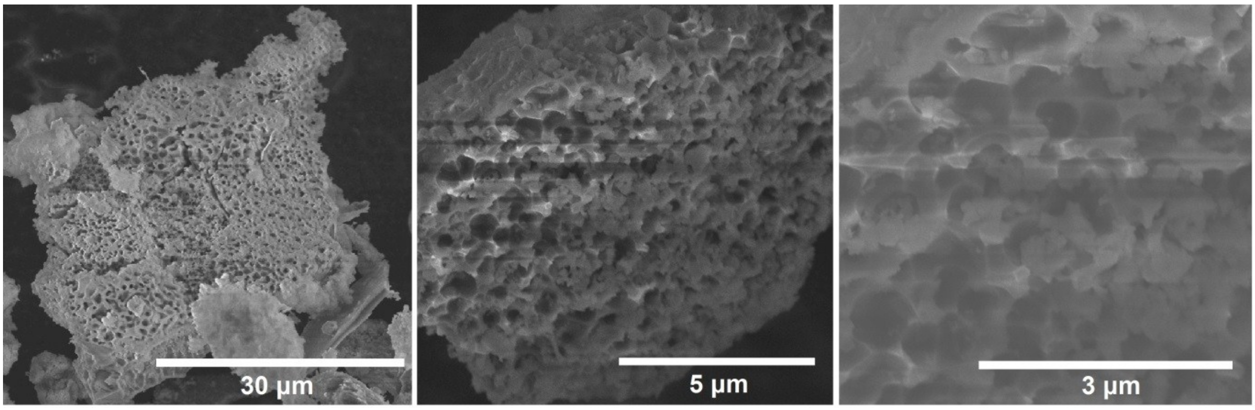

Fig. S2. SEM micrographs of NMIS-Si, supporting the morphological features provided in Fig. 2.

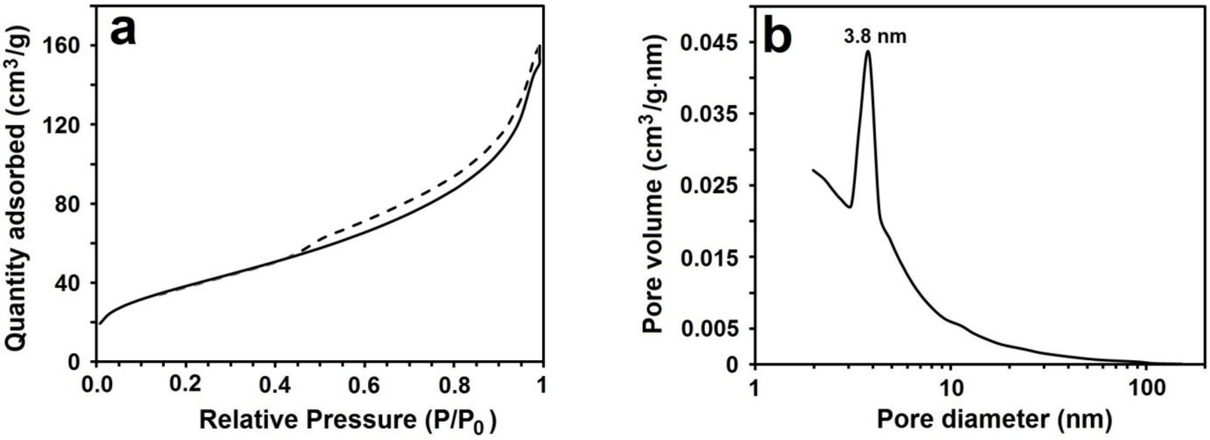

Fig. S3. (a) Nitrogen adsorption–desorption isotherm and (b) pore size distribution of NMIS-Si.

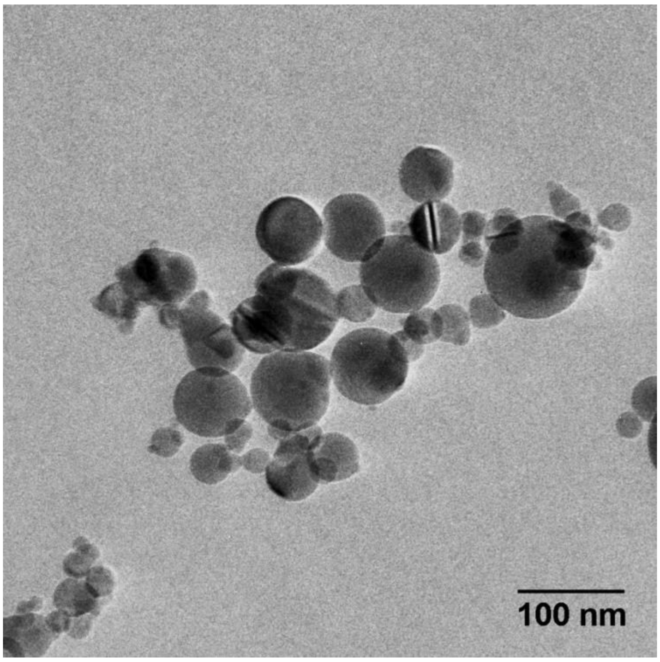

Fig. S4. TEM micrograph of the commercial Si nanoparticles used in this study. This Si material was produced by a laser pyrolysis technique using gaseous SiH_4.

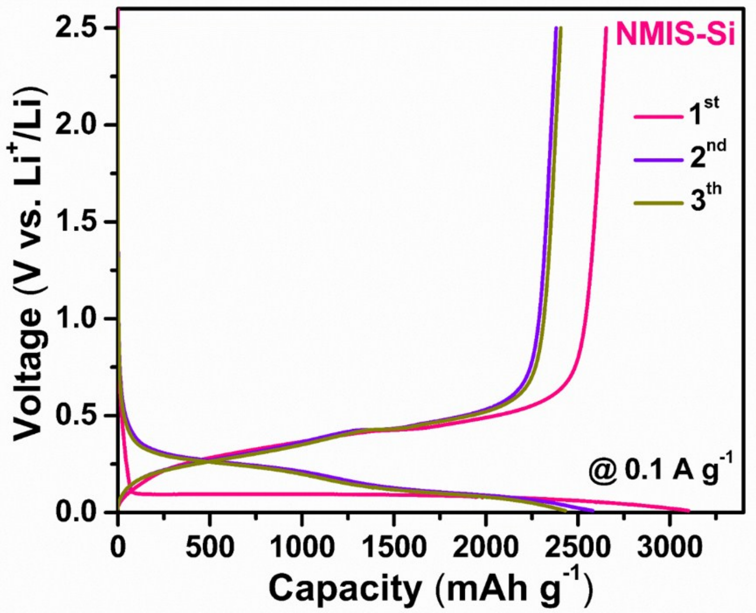

Fig. S5. Charge–discharge voltage profiles for the first three cycles of the NMIS-Si at a current density of 0.10 A g^{-1}

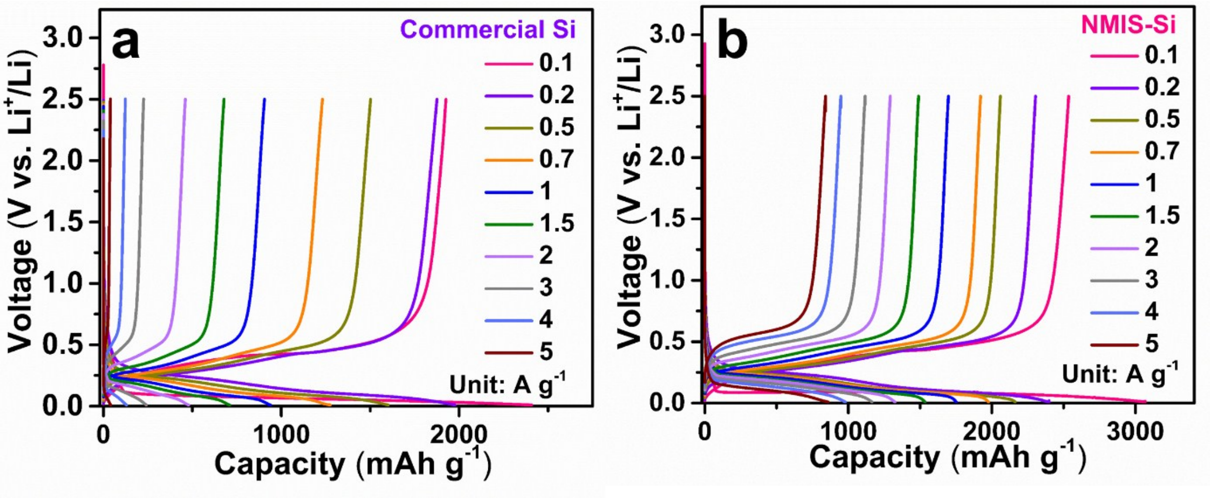

Fig. S6. Charge–discharge voltage profiles of (a) commercial Si and (b) NMIS-Si electrodes at various current densities.

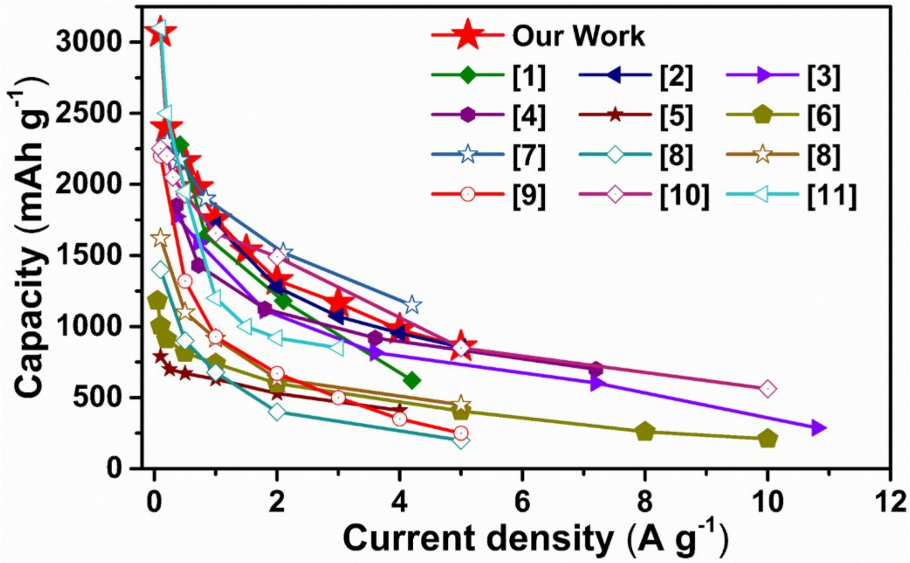

Fig. S7. The capacity of the target NMIS-Si in comparison with those of state-of-the-art porous Si-based LIB anodes reported in the literature (Refs. [1-11]).

The excellent kinetics of the NMIS-Si electrode could be understood from impedance spectroscopy measurements performed after different cycles at selected voltages in the range of 0.01–2.50 V vs. Li. Fig. S8 presents the Nyquist plots of the 1st, 2nd, and 100th cycles. As exhibited in Fig. S8g, the impedance data were fitted to an adequate equivalent circuit model consisting of an initial resistance (R_e), two semicircles at high- and medium-frequency areas (R_{SEI} and R_{ct}, respectively), and a straight line in the low-frequency region known as Warburg impedance (Z_w). R_{SEI} attributes to the Li^+ ions transportation through the SEI layer, and R_{ct} associates with the charge-transfer resistance at the electrode-electrolyte interfaces. Furthermore, the slope of the Nyquist plots at the low frequency region corresponds to the diffusive resistance of Li^+ ions in the electrode. It can be observed from Fig. S8a that the values of R_{SEI} and Rct at the 1st cycle gradually increase during the first discharge to 0.22 V at different discharge states. This general rise in resistance is principally on account of the electrolyte decomposition on the electrode surface, resulting in the formation of insulating SEI layers on the electrode. The subsequent first charging process to 2.50 V (Fig. S8b) resulted in a slight decrease in values of both R_{SEI} and R_{ct}, suggesting that the pulverization of Si nanoparticles is tolerable (Fig. 4f), and thus, the SEI layer is sufficiently thin to grant the ease of Li^+ ions transfer through the formed SEI film, resulting in the enhanced electrochemical performance of the electrode. The resistance values during the 2nd-100th discharge-charge cycles consistently decreased, revealing the formation of a stable and thin SEI layer, and an enhanced charge transport process during the lithiation-delithiation cycles.

Direct in situ high-resolution transmission electron microscopy observation of the lithiation/delithiation process of the NMIS-Si electrode may provide further insights into the electrochemical performance of the nanostructured Si material in future investigations.

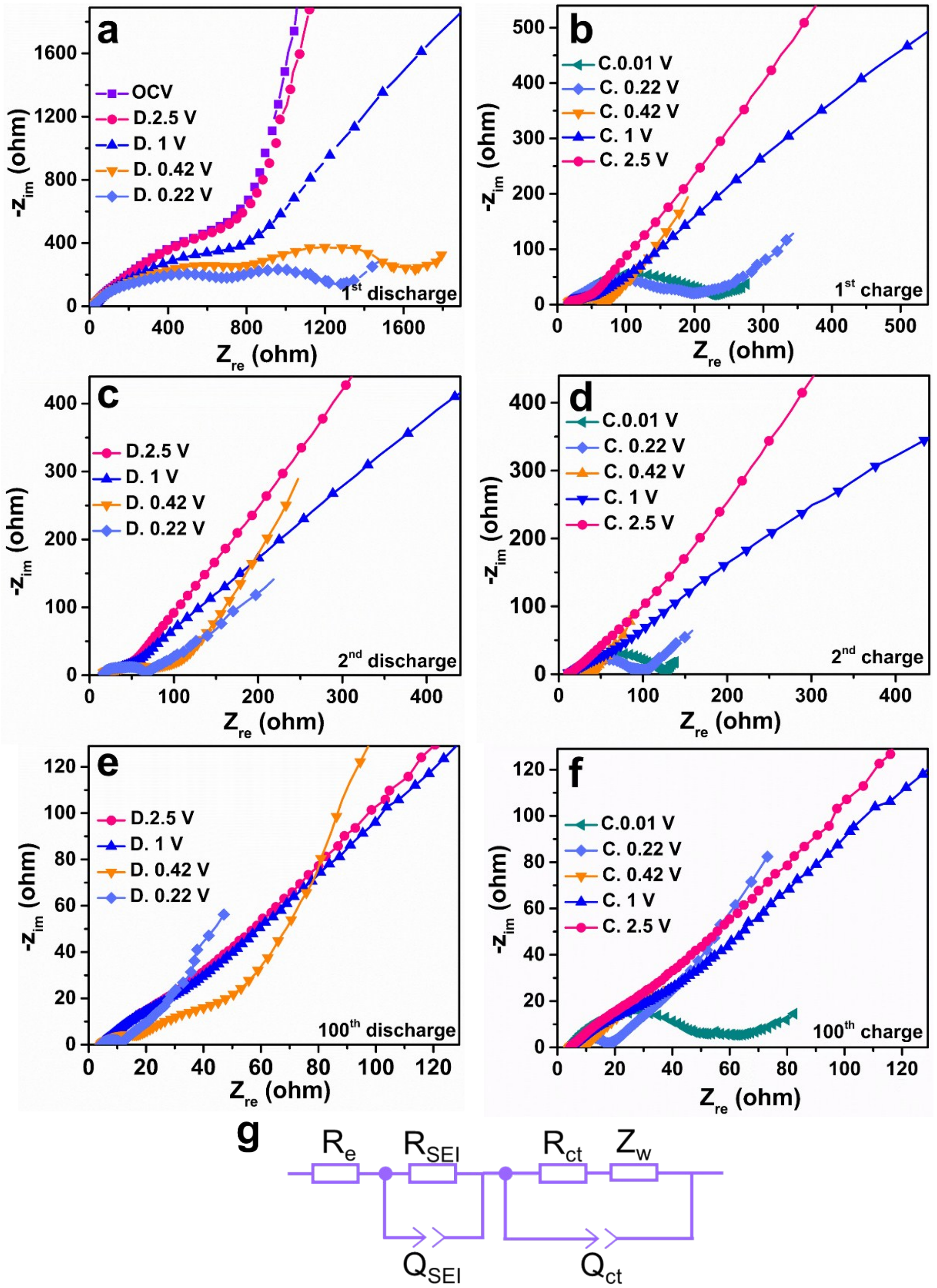

Fig. S8. Nyquist plots of the NMIS-Si electrode at various voltages during the (a,b) 1st, (c,d) 2nd, and (e,f) 100th discharge and charge cycles. (g) Equivalent circuit used for fitting the impedance spectra.

References

[1] H. Zhang, X. Zhang, H. Jin, P. Zong, Y. Bai, K. Lian, H. Xu, F. Ma, Chem. Eng. J. 2018, DOI 10.1016/j.cej.2018.07.054.

[2] Y. An, H. Fei, G. Zeng, L. Ci, S. Xiong, J. Feng, Y. Qian, ACS Nano 2018, 12, 4993.

[3] J. Liang, X. Li, Q. Cheng, Z. Hou, L. Fan, Y. Zhu, Y. Qian, Nanoscale 2015, 7, 3440.

[4] Q. Xiao, M. Gu, H. Yang, B. Li, C. Zhang, Y. Liu, F. Liu, F. Dai, L. Yang, Z. Liu, X. Xiao, G. Liu, P. Zhao, S. Zhang, C. Wang, Y. Lu, M. Cai, Nat. Commun. 2015, 6, 8844.

[5] X. Li, M. Gu, S. Hu, R. Kennard, P. Yan, X. Chen, C. Wang, M. J. Sailor, J.-G. Zhang, J. Liu, Nat. Commun. 2014, 5, 4105.

[6] H. Tian, X. Tan, F. Xin, C. Wang, W. Han, Nano Energy 2015, 11, 490.

[7] S. Kang, K. Yang, S. R. White, N. R. Sottos, Adv. Energy Mater. 2017, 7, 1700045.

[8] N. Kim, H. Park, N. Yoon, J. K. Lee, ACS Nano 2018, 12, 3853.

[9] L. Pan, H. Wang, D. Gao, S. Chen, L. Tan, L. Li, Chem. Commun. 2014, 50, 5878.

[10] Y. Liu, Z. Tai, T. Zhou, V. Sencadas, J. Zhang, L. Zhang, K. Konstantinov, Z. Guo, H.-K. Liu, Adv. Mater. 2017, 29, 1703028.

[11] X. Ding, X. Liu, Y. Huang, X. Zhang, Q. Zhao, X. Xiang, G. Li, P. He, Z. Wen, J. Li, Y. Huang, Nano Energy 2016, 27, 647.